CLNS 00/1691
CLEO 00-18

Study of χ_{c1} and χ_{c2} meson production in B meson decays

CLEO Collaboration

(September 19, 2000)

Abstract

Using a sample of 9.7×10^6 $B\overline{B}$ meson pairs collected with the CLEO detector, we study B decays to the χ_{c1} and χ_{c2} charmonia states, which are reconstructed via their radiative decays to J/ψ. We first measure the branching fraction for inclusive χ_{c1} production in B decays to be $\mathcal{B}(B \to \chi_{c1}X) = (4.14 \pm 0.31 \pm 0.40) \times 10^{-3}$, where the first uncertainty is statistical and the second one is systematic. We derive the branching fractions for direct χ_{c1} and χ_{c2} production in B decays by subtracting the known contribution of the decay chain $B \to \psi(2S)X$ with $\psi(2S) \to \chi_{c1,2}\gamma$. We obtain $\mathcal{B}[B \to \chi_{c1}(\text{direct})X] = (3.83 \pm 0.31 \pm 0.40) \times 10^{-3}$. No statistically significant signal for χ_{c2} production is observed in either case. Using the Feldman-Cousins approach, we determine the 95% confidence intervals to be $[0.2, 2.0] \times 10^{-3}$ for $\mathcal{B}(B \to \chi_{c2}X)$, $[0.0, 1.7] \times 10^{-3}$ for $\mathcal{B}[B \to \chi_{c2}(\text{direct})X]$, and $[0.00, 0.44]$ for the ratio $\Gamma[B \to \chi_{c2}(\text{direct})X]/\Gamma[B \to \chi_{c1}(\text{direct})X]$. We also measure the branching ratio $\Gamma[B \to \chi_{c2}(\text{direct})X_s]/\Gamma[B \to \chi_{c1}(\text{direct})X_s]$ for different X_s configurations by reconstructing B decays into exclusive final states with J/ψ, γ, a kaon, and up to four pions. For all the X_s configurations we observe a strong χ_{c1} signal yet no statistically significant χ_{c2} signal. We discuss how our results compare with theoretical predictions in different models of charmonium production.

S. Chen,[1] J. Fast,[1] J. W. Hinson,[1] J. Lee,[1] D. H. Miller,[1] E. I. Shibata,[1] I. P. J. Shipsey,[1] V. Pavlunin,[1] D. Cronin-Hennessy,[2] A.L. Lyon,[2] E. H. Thorndike,[2] V. Savinov,[3] T. E. Coan,[4] V. Fadeyev,[4] Y. S. Gao,[4] Y. Maravin,[4] I. Narsky,[4] R. Stroynowski,[4] J. Ye,[4] T. Wlodek,[4] M. Artuso,[5] R. Ayad,[5] C. Boulahouache,[5] K. Bukin,[5] E. Dambasuren,[5] S. Karamov,[5] G. Majumder,[5] G. C. Moneti,[5] R. Mountain,[5] S. Schuh,[5] T. Skwarnicki,[5] S. Stone,[5] J.C. Wang,[5] A. Wolf,[5] J. Wu,[5] S. Kopp,[6] M. Kostin,[6] A. H. Mahmood,[7] S. E. Csorna,[8] I. Danko,[8] K. W. McLean,[8] Z. Xu,[8] R. Godang,[9] G. Bonvicini,[10] D. Cinabro,[10] M. Dubrovin,[10] S. McGee,[10] G. J. Zhou,[10] E. Lipeles,[11] S. P. Pappas,[11] M. Schmidtler,[11] A. Shapiro,[11] W. M. Sun,[11] A. J. Weinstein,[11] F. Würthwein,[11,*] D. E. Jaffe,[12] G. Masek,[12] H. P. Paar,[12] E. M. Potter,[12] S. Prell,[12] D. M. Asner,[13] A. Eppich,[13] T. S. Hill,[13] R. J. Morrison,[13] R. A. Briere,[14] G. P. Chen,[14] A. Gritsan,[15] J. P. Alexander,[16] R. Baker,[16] C. Bebek,[16] B. E. Berger,[16] K. Berkelman,[16] F. Blanc,[16] V. Boisvert,[16] D. G. Cassel,[16] P. S. Drell,[16] J. E. Duboscq,[16] K. M. Ecklund,[16] R. Ehrlich,[16] A. D. Foland,[16] P. Gaidarev,[16] L. Gibbons,[16] B. Gittelman,[16] S. W. Gray,[16] D. L. Hartill,[16] B. K. Heltsley,[16] P. I. Hopman,[16] L. Hsu,[16] C. D. Jones,[16] D. L. Kreinick,[16] M. Lohner,[16] A. Magerkurth,[16] T. O. Meyer,[16] N. B. Mistry,[16] E. Nordberg,[16] M. Palmer,[16] J. R. Patterson,[16] D. Peterson,[16] D. Riley,[16] A. Romano,[16] J. G. Thayer,[16] D. Urner,[16] B. Valant-Spaight,[16] G. Viehhauser,[16] A. Warburton,[16] P. Avery,[17] C. Prescott,[17] A. I. Rubiera,[17] H. Stoeck,[17] J. Yelton,[17] G. Brandenburg,[18] A. Ershov,[18] D. Y.-J. Kim,[18] R. Wilson,[18] H. Yamamoto,[19] T. Bergfeld,[20] B. I. Eisenstein,[20] J. Ernst,[20] G. E. Gladding,[20] G. D. Gollin,[20] R. M. Hans,[20] E. Johnson,[20] I. Karliner,[20] M. A. Marsh,[20] C. Plager,[20] C. Sedlack,[20] M. Selen,[20] J. J. Thaler,[20] J. Williams,[20] K. W. Edwards,[21] R. Janicek,[22] P. M. Patel,[22] A. J. Sadoff,[23] R. Ammar,[24] A. Bean,[24] D. Besson,[24] X. Zhao,[24] S. Anderson,[25] V. V. Frolov,[25] Y. Kubota,[25] S. J. Lee,[25] R. Mahapatra,[25] J. J. O'Neill,[25] R. Poling,[25] T. Riehle,[25] A. Smith,[25] C. J. Stepaniak,[25] J. Urheim,[25] S. Ahmed,[26] M. S. Alam,[26] S. B. Athar,[26] L. Jian,[26] L. Ling,[26] M. Saleem,[26] S. Timm,[26] F. Wappler,[26] A. Anastassov,[27] E. Eckhart,[27] K. K. Gan,[27] C. Gwon,[27] T. Hart,[27] K. Honscheid,[27] D. Hufnagel,[27] H. Kagan,[27] R. Kass,[27] T. K. Pedlar,[27] H. Schwarthoff,[27] J. B. Thayer,[27] E. von Toerne,[27] M. M. Zoeller,[27] S. J. Richichi,[28] H. Severini,[28] P. Skubic,[28] and A. Undrus[28]

[1]Purdue University, West Lafayette, Indiana 47907
[2]University of Rochester, Rochester, New York 14627
[3]Stanford Linear Accelerator Center, Stanford University, Stanford, California 94309
[4]Southern Methodist University, Dallas, Texas 75275
[5]Syracuse University, Syracuse, New York 13244
[6]University of Texas, Austin, TX 78712
[7]University of Texas - Pan American, Edinburg, TX 78539
[8]Vanderbilt University, Nashville, Tennessee 37235
[9]Virginia Polytechnic Institute and State University, Blacksburg, Virginia 24061
[10]Wayne State University, Detroit, Michigan 48202
[11]California Institute of Technology, Pasadena, California 91125

[*]Permanent address: Massachusetts Institute of Technology, Cambridge, MA 02139.

[12]University of California, San Diego, La Jolla, California 92093
[13]University of California, Santa Barbara, California 93106
[14]Carnegie Mellon University, Pittsburgh, Pennsylvania 15213
[15]University of Colorado, Boulder, Colorado 80309-0390
[16]Cornell University, Ithaca, New York 14853
[17]University of Florida, Gainesville, Florida 32611
[18]Harvard University, Cambridge, Massachusetts 02138
[19]University of Hawaii at Manoa, Honolulu, Hawaii 96822
[20]University of Illinois, Urbana-Champaign, Illinois 61801
[21]Carleton University, Ottawa, Ontario, Canada K1S 5B6
and the Institute of Particle Physics, Canada
[22]McGill University, Montréal, Québec, Canada H3A 2T8
and the Institute of Particle Physics, Canada
[23]Ithaca College, Ithaca, New York 14850
[24]University of Kansas, Lawrence, Kansas 66045
[25]University of Minnesota, Minneapolis, Minnesota 55455
[26]State University of New York at Albany, Albany, New York 12222
[27]Ohio State University, Columbus, Ohio 43210
[28]University of Oklahoma, Norman, Oklahoma 73019

The recent measurements of charmonium production in various high-energy physics reactions have brought welcome surprises and challenged our understanding both of heavy-quark production and of quarkonium bound state formation. The CDF and D0 measurements [1] of a large production rate for charmonium at high transverse momenta (P_T) were in sharp disagreement with the then-standard color-singlet model. The development of the NRQCD factorization framework [2] has put the calculations of the inclusive charmonium production on a rigorous footing. The high-P_T charmonium production rate at the Tevatron is now well understood in this formalism. The recent CDF measurement of charmonium polarization [3], however, appears to disagree with the NRQCD prediction. The older color-evaporation model accommodates both the high-P_T charmonium production rate and polarization measurements at the Tevatron [4].

Inclusive B decays to charmonia offer another means by which theoretical predictions may be confronted with experimental data. The color-singlet contribution, for example, is thought to be [5] a factor of 5–10 below the observed inclusive J/ψ production rate [6]. A measurement of the χ_{c2}-to-χ_{c1} production ratio in B decays provides an especially clean test of charmonium production models. The $V-A$ current $\overline{c}\gamma_\mu(1-\gamma_5)c$ cannot create a $c\overline{c}$ pair in a ${}^{2S+1}L_J = {}^3P_2$ state, therefore the decay $B \to \chi_{c2}X$ is forbidden at leading order in α_s in the color-singlet model [7]. The importance of the color-octet mechanism for χ_c production in B decays was recognized [8] even before the development of the NRQCD framework [2]. While the NRQCD calculations cannot yet produce sharp quantitative predictions for the χ_{c2}-to-χ_{c1} production ratio in B decays [5], we can consider two limiting cases. If the color-octet mechanism dominates in $B \to \chi_{cJ}X$ decays, then the χ_{c2}-to-χ_{c1} production ratio should be 5:3 because the color-octet contribution is proportional to $2J+1$. In contrast, if the color-singlet contribution dominates, then χ_{c2} production should be strongly suppressed relative to χ_{c1} production. The color-evaporation model predicts the ratio to be $5:3$ [9].

Our data were collected at the Cornell Electron Storage Ring (CESR) with two configurations of the CLEO detector called CLEO II [10] and CLEO II.V [11]. The components of the CLEO detector most relevant to this analysis are the charged particle tracking system, the CsI electromagnetic calorimeter, the time-of-flight system, and the muon chambers. In CLEO II the momenta of charged particles are measured in a tracking system consisting of a 6-layer straw tube chamber, a 10-layer precision drift chamber, and a 51-layer main drift chamber, all operating inside a 1.5 T solenoidal magnet. The main drift chamber also provides a measurement of the specific ionization, dE/dx, used for particle identification. For CLEO II.V, the straw tube chamber was replaced with a 3-layer silicon vertex detector, and the gas in the main drift chamber was changed from an argon-ethane to a helium-propane mixture. The muon chambers consist of proportional counters placed at increasing depths in the steel absorber.

We use 9.2 fb^{-1} of e^+e^- data taken at the $\Upsilon(4S)$ resonance and 4.6 fb^{-1} taken 60 MeV below the $\Upsilon(4S)$ resonance (off-$\Upsilon(4S)$ sample). Two thirds of the data were collected with the CLEO II.V detector. The simulated event samples used in this analysis were generated with a GEANT-based [12] simulation of the CLEO detector response and were processed in a manner similar to the data.

We reconstruct the $\chi_{c1,2}$ radiative decays to J/ψ. The branching fractions for the $\chi_{c1,2} \to J/\psi\,\gamma$ decays are, respectively, $(27.3\pm1.6)\%$ and $(13.5\pm1.1)\%$, whereas the branching fraction for the $\chi_{c0} \to J/\psi\,\gamma$ decay is only $(0.66 \pm 0.18)\%$ [14]. In addition, the χ_{c0} production rate in B decays is expected to be smaller than the $\chi_{c1,2}$ rates [5,8]. We therefore do not attempt to measure χ_{c0} production in this analysis.

The J/ψ reconstruction procedure is described in Ref. [13] and summarized here. We reconstruct both $J/\psi \to \mu^+\mu^-$ and $J/\psi \to e^+e^-$ decays, recovering the bremsstrahlung photons for the $J/\psi \to e^+e^-$ mode. We use the normalized invariant mass for the J/ψ candidate selection (Fig.1 of Ref. [13]). For example, the normalized $J/\psi \to \mu^+\mu^-$ mass is defined as $[M(\mu^+\mu^-) - M_{J/\psi}]/\sigma(M)$, where $M_{J/\psi}$ is the world average value of the J/ψ mass [14] and $\sigma(M)$ is the expected mass resolution for that particular $\mu^+\mu^-$ combination calculated from track four-momentum covariance matrices. We require the normalized mass to be between -6 and $+3$ for the $J/\psi \to e^+e^-$ candidates and between -4 and $+3$ for the $J/\psi \to \mu^+\mu^-$ candidates. The momentum of the J/ψ candidates is required to be less than 2 GeV/c, which is slightly above the maximal J/ψ momentum in B decays.

Photon candidates for $\chi_{c1,2} \to J/\psi\,\gamma$ reconstruction must be detected in the central angular region of the calorimeter ($|\cos\theta_\gamma| < 0.71$), where our detector has the best energy resolution. Most of the photons in $\Upsilon(4S) \to B\overline{B}$ events come from π^0 decays. We therefore discard those photon candidates which, when paired with another γ in the event, produce a normalized $\pi^0 \to \gamma\gamma$ mass between -3 and $+2$.

In the first part of this work, called the inclusive analysis, we investigate $B \to \chi_{c1,2}X$ decays reconstructing only J/ψ and γ. We determine the χ_{c1} and χ_{c2} yields in a binned maximum-likelihood fit to the mass-difference distribution $M(J/\psi\gamma) - M(J/\psi)$ (Fig. 1a), where $M(J/\psi)$ is the measured mass of a J/ψ candidate. The excellent electromagnetic calorimeter allows us to resolve the χ_{c1} and χ_{c2} peaks. The $M(J/\psi\gamma) - M(J/\psi)$ mass-difference resolution is 8 MeV/c^2 and is dominated by the photon energy resolution. The bin width in the fit is 1 MeV/c^2. The background in the fit is approximated by a 5th-order Chebyshev polynomial, chosen as the minimal-order polynomial well fitting the background in a high-statistics sample of simulated $\Upsilon(4S) \to B\overline{B}$ events. All the polynomial coefficients are allowed to float in the fit. The χ_{c1} and χ_{c2} signal shapes are fit with templates extracted from Monte Carlo simulation; only the template normalizations are free in the fit. The χ_{c1} and χ_{c2} signal yields in the $\Upsilon(4S)$ data are $N^{\mathrm{ON}}(\chi_{c1}) = 672 \pm 47(\mathrm{stat})$ and $N^{\mathrm{ON}}(\chi_{c2}) = 83 \pm 37(\mathrm{stat})$. The χ_{c1} and χ_{c2} yields in off-$\Upsilon(4S)$ data are both consistent with zero: $N^{\mathrm{OFF}}(\chi_{c1}) = 4 \pm 7(\mathrm{stat})$ and $N^{\mathrm{OFF}}(\chi_{c2}) = 1 \pm 7(\mathrm{stat})$. Subtracting the contributions from non-$B\overline{B}$ continuum events, we obtain the total inclusive $B \to \chi_{c1}X$ and $B \to \chi_{c2}X$ event yields $N(B \to \chi_{c1}X) = 664 \pm 49(\mathrm{stat})$ and $N(B \to \chi_{c2}X) = 81 \pm 39(\mathrm{stat})$.

Taking into account the systematic uncertainties associated with the fit, we determine the $B \to \chi_{c2}X$ signal yield significance to be 2.0 standard deviations (σ). Subtracting the known contribution of the decay chain $B \to \psi(2S)X$ with $\psi(2S) \to \chi_{c2}\gamma$ and accounting for the associated systematic uncertainty, we likewise determine the significance of the evidence for the decay $B \to \chi_{c2}(\mathrm{direct})X$ to be only 1.4σ.

To calculate the branching fractions $\mathcal{B}(B \to \chi_{c1,2}X)$, we use the measured signal yields $N(B \to \chi_{c1,2}X)$, the reconstruction efficiencies, the number of produced $B\overline{B}$ pairs, and the daughter branching fractions. The reconstruction efficiencies, determined from simulation, are $(25.7 \pm 0.2)\%$ for χ_{c1} and $(26.6 \pm 0.2)\%$ for χ_{c2}, where the uncertainties are due to the size of our $B \to \chi_{c1,2}X$ simulation samples. For the calculation of the rates for the decays $B \to \chi_{c1,2}(\mathrm{direct})X$, we make an assumption that the only other source of $\chi_{c1,2}$ production in B decays is the decay chain $B \to \psi(2S)X$ with $\psi(2S) \to \chi_{c1,2}\gamma$. The 95% confidence intervals are calculated using the Feldman-Cousins approach [16]. The resulting branching fractions are listed in Table I. Taking into account correlations between the uncertainties, we obtain the branching ratio $\Gamma[B \to \chi_{c2}(\mathrm{direct})X]/\Gamma[B \to \chi_{c1}(\mathrm{direct})X] = 0.18 \pm 0.13 \pm 0.04$; the 95% CL upper limit on the ratio is 0.44.

TABLE I. Branching fractions for inclusive B decays to χ_{c1} and χ_{c2}.

Branching fraction	Measured value ($\times 10^{-3}$)	95% CL interval ($\times 10^{-3}$)
$\mathcal{B}(B \to \chi_{c1}X)$	$4.14 \pm 0.31 \pm 0.40$	—
$\mathcal{B}[B \to \chi_{c1}(\mathrm{direct})X]$	$3.83 \pm 0.31 \pm 0.40$	—
$\mathcal{B}(B \to \chi_{c2}X)$	$0.98 \pm 0.48 \pm 0.15$	$[0.2, 2.0]$
$\mathcal{B}[B \to \chi_{c2}(\mathrm{direct})X]$	$0.71 \pm 0.48 \pm 0.16$	$[0.0, 1.7]$

The systematic uncertainties are listed in Table II. The sources of the uncertainty can be grouped into three categories:

Fit procedure.— This category includes the uncertainties due to our choice of the signal and background shapes as well as the bin size. To fit the χ_{c1} and χ_{c2} signal, we use the templates extracted from simulation. We therefore are sensitive to imperfections in the simulation of the photon energy measurement. The systematic uncertainties associated with the simulation of the calorimeter response are estimated by comparing the $\pi^0 \to \gamma\gamma$ invariant mass lineshapes for inclusive π^0 candidates in the data and in Monte Carlo samples. Then the χ_{c1} and χ_{c2} templates are modified accordingly in order to determine the resulting uncertainty in the signal yields. To estimate the uncertainty associated with the calorimeter energy scale, we shift the χ_{c1} and χ_{c2} templates by ± 0.6 MeV/c^2 in the fit. The uncertainty due to time-dependent variations of the calorimeter energy scale is small compared to the overall energy scale uncertainty. To estimate the uncertainty due to the calorimeter energy resolution, we change the width of the χ_{c1} and χ_{c2} templates by $\pm 4\%$. The uncertainty in the background shape is probed by fitting the background with a template extracted from high-statistics samples of simulated $\Upsilon(4S) \to B\overline{B}$ and non-$B\overline{B}$ continuum events; only the template normalization, not its shape, is allowed to float in the fit.

Efficiency calculation.— This category includes the uncertainties in the number of produced $B\overline{B}$ pairs, tracking efficiency, photon detection efficiency, lepton detection efficiency, and model-dependence and statistical uncertainty of the $B \to \chi_{c1,2}X$ simulation. The $\chi_{c1,2}$ polarization affects the photon energy spectrum. We define the helicity angle θ_h to be the angle between the γ direction in χ_c frame and the χ_c direction in the B frame. We assume a flat $\cos\theta_h$ distribution in our simulation. The systematic uncertainty associated with this assumption is estimated by comparing the reconstruction efficiencies in the Monte Carlo samples with $I(\theta_h) \propto \sin^2\theta_h$ and $I(\theta_h) \propto \cos^2\theta_h$ angular distributions. Parity is conserved in the decays $\chi_{c1,2} \to J/\psi\gamma$, so the helicity angle distribution contains only even powers of $\cos\theta_h$. Another source of uncertainty is our modeling of the X system in the $B \to \chi_{c1,2}X$ simulation. Photon detection efficiency depends on the assumed model through the χ_c momentum spectrum and the π^0 multiplicity of the final state. In our simulation, we assume that X is either a single K or one of the higher K resonances; we also include the decay chain

$B \to \psi(2S)X$ with $\psi(2S) \to \chi_{c1,2}\gamma$. To estimate the systematic uncertainty, we compare the $\chi_c \to J/\psi\gamma$ detection efficiency extracted using this sample with the efficiency in the sample where we assume that X is either a $K^{\pm}$ or $K^0_S \to \pi^+\pi^-$.

Assumed branching fractions.— This category includes the uncertainties on the external branching fractions. We use the following values of the daughter branching fractions: $\mathcal{B}(J/\psi \to \ell^+\ell^-) = (5.894 \pm 0.086)\%$ [15], $\mathcal{B}(\chi_{c1} \to J/\psi\gamma) = (27.3 \pm 1.6)\%$ [14], and $\mathcal{B}(\chi_{c2} \to J/\psi\gamma) = (13.5 \pm 1.1)\%$ [14]. In the calculation of $\mathcal{B}[B \to \chi_{c1,2}(\text{direct})X]$, we also assume the following values: $\mathcal{B}(B \to \psi(2S)X) = (3.5 \pm 0.5) \times 10^{-3}$ [14], $\mathcal{B}(\psi(2S) \to \chi_{c1}\gamma) = (8.7 \pm 0.8)\%$ [14], and $\mathcal{B}(\psi(2S) \to \chi_{c2}\gamma) = (7.8 \pm 0.8)\%$ [14].

TABLE II. Systematic uncertainties on $\mathcal{B}(B \to \chi_{c1,2}X)$.

Source of systematic uncertainty	relative uncertainty in % $\mathcal{B}(B \to \chi_{c1}X)$	$\mathcal{B}(B \to \chi_{c2}X)$
Fit procedure		
γ energy scale	0.4	5.6
γ energy resolution	2.8	6.9
Background shape	1.8	6.8
Bin size	0.0	1.9
Efficiency calculation		
$N(B\overline{B})$	2.0	2.0
Tracking efficiency	2.0	2.0
Lepton identification	4.2	4.2
Photon finding	2.5	2.5
Monte Carlo statistics	0.7	0.7
Model for X in $B \to \chi_{c1,2}X$	3.3	3.3
Polarization of $\chi_{c1,2}$	1.0	1.0
Assumed branching fractions		
$\mathcal{B}(\chi_{c1,2} \to J/\psi\gamma)$	5.9	8.1
$\mathcal{B}(J/\psi \to \ell^+\ell^-)$	1.5	1.5
$\mathcal{B}(B \to \psi(2S)X)$[a]	1.1	5.5
$\mathcal{B}(\psi(2S) \to \chi_{c1,2}\gamma)$[a]	0.7	4.0

[a]Contributes only to uncertainty on $\mathcal{B}[B \to \chi_{c1,2}(\text{direct})X]$.

In the second part of this work, called the B-reconstruction analysis, we employ the B-reconstruction technique similar to the one developed for the $b \to s\gamma$ rate measurement [17]. We still extract χ_{c1} and χ_{c2} signal yields from a fit to $M(J/\psi\gamma) - M(J/\psi)$ distribution, but we select only those $J/\psi\gamma$ combinations that reconstruct to a $B \to J/\psi\gamma X_s$ decay. This B-reconstruction technique is used to suppress backgrounds and allows us to probe the composition of the X_s system accompanying $\chi_{c1,2}$ mesons. We extract the branching ratio $\mathcal{R}(\chi_{c2}/\chi_{c1}) \equiv \Gamma[B \to \chi_{c2}(\text{direct})X_s]/\Gamma[B \to \chi_{c1}(\text{direct})X_s]$ for the following three X_s configurations:

1. *Sample A.*— X_s is reconstructed as a kaon (K^+ or $K^0_S \to \pi^+\pi^-$) with 0 to 4 pions, one of which can be a π^0. We consider 21 possible X_s modes as well as the charge conjugates of these modes.

2. *Sample B.*— X_s is reconstructed as a single kaon or $K^*(892)$. A $K\pi$ combination is a K^* candidate if $|M(K\pi) - M_{K^*}| < 75\ \ \mathrm{MeV}/c^2$, where M_{K^*} is the world average $K^*(892)$ mass [14].

3. *Sample C.*— X_s is reconstructed as a kaon with 1 to 4 pions, but not as a $K^*(892)$ candidate ($|M(K\pi) - M_{K^*}| > 200\ \ \mathrm{MeV}/c^2$).

Thus samples B and C are subsets of A. To an excellent approximation, sample A is a sum of B and C. With sample A, we try to reconstruct as many $B \to J/\psi\gamma X_s$ decays as possible. Dividing sample A into subsamples B and C, we also probe the dynamics of the $B \to \chi_{c1,2}X_s$ decays. If the dominant production mechanisms for χ_{c1} and χ_{c2} are different, color-singlet mechanism for χ_{c1} and color-octet for χ_{c2}, then it is natural to expect that χ_{c2}, in comparison with χ_{c1}, is more often accompanied by multi-body X_s states rather than a single K or K^*. Thus the measured χ_{c2}-to-χ_{c1} production ratio might be quite different for samples B and C.

We require that the charged kaon and pion candidates have, if available, dE/dx and time-of-flight measurements that lie within 3σ of the expected values. The dE/dx measurement is required for kaons, but used only if available for pions. The time-of-flight measurement is used only if available. The $K^0_S \to \pi^+\pi^-$ candidates are selected from pairs of tracks forming displaced vertices. We require the absolute value of the normalized $K^0_S \to \pi^+\pi^-$ mass to be less than 4 and perform a fit constraining the mass of each K^0_S candidate to the world average value [14]. Photon candidates for $\pi^0 \to \gamma\gamma$ decays are required to have an energy of at least 30 MeV in the central region and at least 50 MeV in the endcap region ($0.71 < |\cos\theta_\gamma| < 0.95$) of the calorimeter. We require the absolute value of the normalized $\pi^0 \to \gamma\gamma$ mass to be less than 3 and perform a fit constraining the mass of each π^0 candidate to the world average value [14]. The J/ψ four-momentum used in $B \to J/\psi\gamma X_s$ reconstruction is obtained by performing a fit constraining the J/ψ candidate mass to the world average value [14].

The B candidates are selected by means of two observables. The first observable is the difference between the energy of the B candidate and the beam energy, $\Delta E \equiv E(B) - E_{\mathrm{beam}}$. The average ΔE resolution varies from 12 to 17 MeV depending on the B-reconstruction mode. The second observable is the beam-constrained B mass, $M(B) \equiv \sqrt{E^2_{\mathrm{beam}} - p^2(B)}$, where $p(B)$ is the B candidate momentum. The average $M(B)$ resolution is 2.7 MeV/c^2 and is dominated by the beam energy spread. We use the normalized $M(B)$ and ΔE variables and require $|\Delta E|/\sigma(\Delta E) < 3$ and $|M(B) - M_B|/\sigma(M) < 3$, where M_B is the nominal B meson mass. The fit to $M(J/\psi\gamma) - M(J/\psi)$ distribution is then performed in the same manner as in the inclusive analysis. We still use a 5th order Chebyshev polynomial to fit the background for samples A and C, but we reduce the order of the polynomial to 3 for the low-statistics sample B. The fits are shown in Fig. 1 and the χ_{c1} and χ_{c2} signal yields are listed in Table III. The B-reconstruction technique renders negligible the contribution from non-$B\overline{B}$ continuum events. We finally subtract the $\psi(2S) \to \chi_{c1,2}\gamma$ feeddown to obtain the rates for direct $\chi_{c1,2}$ production in B decays. For all three X_s configurations, we observe a strong χ_{c1} signal yet no statistically significant signal for direct χ_{c2} production (Table III). To calculate the branching ratio $\mathcal{R}(\chi_{c2}/\chi_{c1})$, we multiply the ratio of the feeddown-corrected $\chi_{c1,2}$ yields by the reconstruction efficiency ratio $\mathcal{E}(\chi_{c1})/\mathcal{E}(\chi_{c2})$ and by the branching ratio

$\Gamma(\chi_{c1} \to J/\psi\gamma)/\Gamma(\chi_{c2} \to J/\psi\gamma)$. The efficiency of the B-reconstruction depends on the composition of the X_s system. We assume that the X_s system composition is the same for χ_{c1} and χ_{c2} production. From our simulation we determine $\mathcal{E}(\chi_{c1})/\mathcal{E}(\chi_{c2}) \simeq 0.93$ for all three X_s configurations. The resulting χ_{c2}-to-χ_{c1} production ratios are listed in Table III.

TABLE III. Results for each of the three X_s configurations used in $B \to J/\psi\gamma X_s$ reconstruction. The χ_{c1} and χ_{c2} event yields with associated statistical uncertainties are listed in lines 1 and 2. Line 3 contains the significance of the $B \to \chi_{c2}(\text{direct})X_s$ signal with statistical and systematic uncertainties taken into account. Lines 4 and 5 contain the measured value and 95% confidence interval for the branching ratio $\mathcal{R}(\chi_{c2}/\chi_{c1}) \equiv \Gamma[B \to \chi_{c2}(\text{direct})X_s]/\Gamma[B \to \chi_{c1}(\text{direct})X_s]$, determined with an assumption that the X_s system composition is the same for χ_{c1} and χ_{c2} production.

	Sample A	Sample B	Sample C
$N(B \to \chi_{c1}X_s)$	279 ± 25	96 ± 12	183 ± 22
$N(B \to \chi_{c2}X_s)$	31^{+18}_{-17}	$13.9^{+7.0}_{-6.2}$	18 ± 16
Significance of $B \to \chi_{c2}(\text{direct})X_s$	1.2σ	2.0σ	0.6σ
$\mathcal{R}(\chi_{c2}/\chi_{c1})$	$0.18 \pm 0.12 \pm 0.09$	$0.27^{+0.15}_{-0.13} \pm 0.05$	$0.14 \pm 0.18 \pm 0.14$
95% CL interval for $\mathcal{R}(\chi_{c2}/\chi_{c1})$	$[0.00, 0.48]$	$[0.04, 0.58]$	$[0.00, 0.59]$

The systematic uncertainties for the B-reconstruction analysis are listed in Table IV. The sources of uncertainty can be grouped into the following four categories:

Fit procedure.— As in the inclusive analysis, we estimate the uncertainties in the signal and background shapes. We shift the $\chi_{c1,2}$ templates by ± 0.6 MeV$/c^2$ and vary their widths by $\pm 4\%$. The requirement on ΔE in $B \to J/\psi\gamma X_s$ reconstruction truncates the low-side tail of the $\chi_{c1,2}$ shapes. We estimate the uncertainty due to this effect by using the $\chi_{c1,2}$ templates obtained from the simulation with a requirement that the measured χ_c energy is within 3σ of the generated value. The uncertainty in the background shape dominates the fit procedure uncertainty. To probe this uncertainty, we fit the background with different templates, allowing only the template normalization, not its shape, to float in the fit. One template is extracted from simulation separately for each of the samples A, B, and C. Another template, the same for all three X_s configurations, is the background shape from the inclusive analysis (Fig. 1a).

$\psi(2S)$ subtraction.— The sources of the systematic uncertainty associated with the $\psi(2S)$-feeddown subtraction include $\mathcal{B}(B \to \psi(2S)X)$, $\mathcal{B}(\psi(2S) \to \chi_{c1,2}\gamma)$, the size of our $B \to \psi(2S)X$ simulation sample, and the composition of X in $B \to \psi(2S)X$ decays. To estimate the uncertainty due to our model of the X system composition in the $B \to \psi(2S)X$ simulation, we check whether the data and the simulation agree on the ratio of $\psi(2S) \to \ell^+\ell^-$ event yields obtained in the inclusive reconstruction and after the $B \to \psi(2S)X_s$ reconstruction. This category also includes the uncertainties that would have canceled for the ratio $\mathcal{R}(\chi_{c2}/\chi_{c1})$ were it not for the $\psi(2S)$-feeddown subtraction. These sources of uncertainty are $\mathcal{B}(J/\psi \to \ell^+\ell^-)$, $N(B\overline{B})$, tracking, photon finding, and lepton identification.

$\mathcal{E}(\chi_{c2})/\mathcal{E}(\chi_{c1})$.— We assume that the X_s system in $B \to \chi_{c1,2}X_s$ is the same for χ_{c1} and χ_{c2}. We do not assign any uncertainty for this assumption. The remaining sources of uncertainty are the $\chi_{c1,2}$ polarization and the statistics of the $B \to \chi_{c1,2}X_s$ simulation samples.

$\mathcal{B}(\chi_{c1,2} \to J/\psi\gamma)$.— Our measurement depends on the ratio $\Gamma(\chi_{c1} \to J/\psi\gamma)/\Gamma(\chi_{c2} \to J/\psi\gamma)$ and its uncertainty.

TABLE IV. The absolute systematic uncertainties on the branching ratio $\mathcal{R}(\chi_{c2}/\chi_{c1})$ for each of the three X_s configurations used in $B \to J/\psi\gamma X_s$ reconstruction.

	uncertainty on $\mathcal{R}(\chi_{c2}/\chi_{c1})$		
Source of uncertainty	Sample A	Sample B	Sample C
Fit procedure	0.084	0.039	0.142
$\psi(2S)$ subtraction	0.007	0.001	0.006
$\mathcal{E}(\chi_{c1})/\mathcal{E}(\chi_{c2})$	0.003	0.006	0.003
$\mathcal{B}(\chi_{c1,2} \to J/\psi\gamma)$	0.022	0.026	0.019
Added in quadrature	0.09	0.05	0.14

In conclusion, we have measured the branching fractions for inclusive B decays to the χ_{c1} and χ_{c2} charmonia states. Our measurements are consistent with and supersede the previous CLEO results [6]. We have also studied $B \to \chi_{c1,2}X_s$ decays, reconstructing X_s as a kaon and up to four pions. In this way, we have measured the branching ratio $\Gamma[B \to \chi_{c2}(\text{direct})X_s]/\Gamma[B \to \chi_{c1}(\text{direct})X_s]$ for three X_s configurations. In all the cases, we observe strong χ_{c1} signal yet no statistically significant signal for χ_{c2} production. Our measurement of the χ_{c2}-to-χ_{c1} production ratio in B decays is consistent with the prediction of the color-singlet model [7] and disagrees with the color-evaporation model [9]. In the NRQCD framework, our measurement suggests that the color-octet mechanism does not dominate in $B \to \chi_c X$ decays.

We gratefully acknowledge the effort of the CESR staff in providing us with excellent luminosity and running conditions. This work was supported by the National Science Foundation, the U.S. Department of Energy, the Research Corporation, the Natural Sciences and Engineering Research Council of Canada, the A.P. Sloan Foundation, the Swiss National Science Foundation, the Texas Advanced Research Program, and the Alexander von Humboldt Stiftung.

REFERENCES

[1] CDF Collaboration, F. Abe *et al.*, Phys. Rev. Lett. **69**, 3704 (1992); **79**, 572 (1997); **79**, 578 (1997); D0 Collaboration, S. Abachi *et al.*, Phys. Lett. B **370**, 239 (1996).

[2] G. T. Bodwin, E. Braaten, and G. P. Lepage, Phys. Rev. D **51**, 1125 (1995).

[3] CDF Collaboration, T. Affolder *et al.*, Report No. FERMILAB-PUB-00-090-E, hep-ex/0004027 (submitted to Phys. Rev. Lett.).

[4] J. F. Amundson *et al.*, Phys. Lett. B **390**, 323 (1997)

[5] M. Beneke, F. Maltoni, and I. Z. Rothstein, Phys. Rev. D **59**, 054003 (1999).

[6] CLEO Collaboration, R. Balest *et al.*, Phys. Rev. D **52**, 2661 (1995).

[7] J. H. Kühn, S. Nussinov, and R. Rückl, Z. Phys. C **5**, 117 (1980); J. H. Kühn and R. Rückl, Phys. Lett. **135B**, 477 (1984); Phys. Lett. B **258**, 499 (1991).

[8] G. T. Bodwin *et al.*, Phys. Rev. D **46**, 3703 (1992).

[9] G. A. Schuler, Eur. Phys. J. C **8**, 273 (1999).

[10] CLEO Collaboration, Y. Kubota *et al.*, Nucl. Instrum. Meth. Phys. Res. A **320**, 66 (1992).

[11] T.S. Hill, Nucl. Instrum. Meth. Phys. Res. A **418**, 32 (1998).

[12] CERN Program Library Long Writeup W5013 (1993).

[13] CLEO Collaboration, P. Avery *et al.*, Phys. Rev. D **62**, 051101 (2000)

[14] Particle Data Group, D.E. Groom *et al.*, Eur. Phys. J. C **15**, 1 (2000).

[15] BES Collaboration, J. Z. Bai *et al.*, Phys. Rev. D **58**, 092006 (1998).

[16] G.J. Feldman and R.D. Cousins, Phys. Rev. D **57**, 3873 (1998).

[17] CLEO Collaboration, M. S. Alam *et al.*, Phys. Rev. Lett. **74**, 2885 (1995).

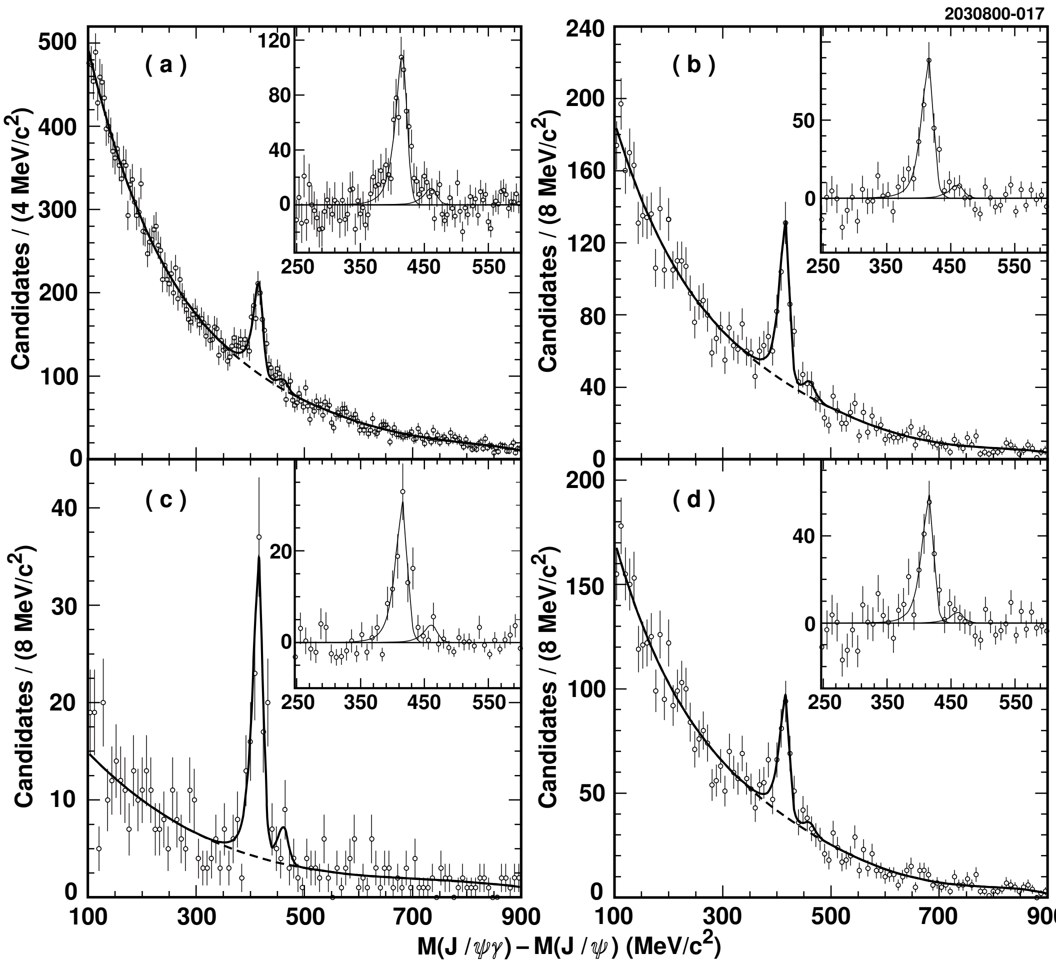

FIG. 1. The $M(J/\psi\gamma) - M(J/\psi)$ distribution in the $\Upsilon(4S)$ data (points with error bars). Plot (a) is for inclusive $J/\psi\gamma$ combinations, whereas plots (b), (c), and (d) are for those $J/\psi\gamma$ combinations that reconstruct to a $B \to J/\psi\gamma X_s$ decay with the X_s composition corresponding to samples A, B, and C described in the text. The fit function is shown by a solid line with the background component represented by a dashed line. The insets show the background-subtracted distributions with the χ_{c1} and χ_{c2} fit components represented by a solid line.